# The response of the Antarctic Circumpolar Current to recent climate change

C. W. BÖNING[1]*, A. DISPERT[1], M. VISBECK[1], S. R. RINTOUL[2] AND F. U. SCHWARZKOPF[1]

[1]Leibniz-Institut für Meereswissenschaften (IFM-GEOMAR), Düsternbrooker Weg 20, 24105 Kiel, Germany

[2]Centre for Australian Weather and Climate Research—a partnership of the Bureau of Meteorology and CSIRO, Wealth from Oceans Flagship, and the Australian Climate and Ecosystems Cooperative Research Centre, Hobart, Tasmania 7000, Australia

*e-mail: cboening@ifm-geomar.de

Published online: 23 November 2008; doi:10.1038/ngeo362

**Observations show a significant intensification of the Southern Hemisphere westerlies, the prevailing winds between the latitudes of 30° and 60° S, over the past decades. A continuation of this intensification trend is projected by climate scenarios for the twenty-first century. The response of the Antarctic Circumpolar Current and the carbon sink in the Southern Ocean to changes in wind stress and surface buoyancy fluxes is under debate. Here we analyse the Argo network of profiling floats and historical oceanographic data to detect coherent hemispheric-scale warming and freshening trends that extend to depths of more than 1,000 m. The warming and freshening is partly related to changes in the properties of the water masses that make up the Antarctic Circumpolar Current, which are consistent with the anthropogenic changes in heat and freshwater fluxes suggested by climate models. However, we detect no increase in the tilt of the surfaces of equal density across the Antarctic Circumpolar Current, in contrast to coarse-resolution model studies. Our results imply that the transport in the Antarctic Circumpolar Current and meridional overturning in the Southern Ocean are insensitive to decadal changes in wind stress.**

The Antarctic Circumpolar Current (ACC) is the dominant feature of ocean circulation in the Southern Hemisphere[1]. Driven at least in part by the vigorous mid-latitude westerly winds, the ACC is associated with strongly tilted surfaces of constant density in the meridional direction. As these provide an effective connection between surface and deep ocean waters, the ACC is of unique importance for air–sea exchanges of heat, fresh water and atmospheric trace gases, and thus for the evolution of climate under increasing greenhouse gas emissions to the atmosphere[2,3]. The ACC regime accounts for a large fraction of global ocean warming[4–7], and for ∼40% of the global oceanic uptake of anthropogenic $CO_2$ over the past two centuries[8,9]. However, model simulations[10–12] suggest that the future of this carbon sink depends rather sensitively on the response of the ACC circulation system to the strengthening of the westerlies projected by IPCC climate scenarios for the twenty-first century[13,14].

Climate model studies show a progressive increase in the tilt of density surfaces across the ACC in response to poleward intensifying westerly winds, relating to an increase in ACC transport and southward shift of its mean position[13,15,16]. The dynamic adjustment of the ACC in these coarse-resolution models is governed by the effect of enhanced northward Ekman fluxes, with an enhanced downwelling of surface waters north of the ACC, and upwelling of deep waters south of the ACC (refs 17–19 ). However, this behaviour is under debate, because the Ekman effect may be opposed by a wind-induced increase in eddy fluxes. High-resolution models with explicit eddies suggest that the increase in northward Ekman transport caused by stronger westerly winds is compensated by southward eddy fluxes, resulting in little change in mean transport and overturning[20–22].

Atmospheric observations and reanalyses indicate a significant intensification of the westerlies in conjunction with the positive trend of the Southern Annular Mode during recent decades[23,24]. While evidence for a response of the ACC eddy activity to inter-annual changes in zonal wind stress is provided by satellite altimeter data[25], understanding of changes in the density structure of the ACC has been hampered by the scarcity of historical measurements in the Southern Ocean. Temperatures recorded in the 1990s by mid-depth autonomous floats[26], and more recently[27] by the profiling floats of the Argo network[28], reveal a systematic warming within the ACC compared with earlier hydrographic measurements. The warming pattern seemed largely consistent with the hypothesis of a wind-forced southward migration of the isopycnal surfaces by about 50 km. However, no studies have yet examined changes in salinity and density for the circumpolar extent of the ACC.

Here we assess the structure of hemispheric-scale density trends across the ACC, using the temperature and salinity profiles provided by Argo floats and a comprehensive compilation of historic data, and we elucidate the nature of the ACC changes by contrasting the trends on isobaric surfaces with the trends in water-mass properties on isopycnal surfaces.

## SPATIAL PATTERN OF CHANGES ALONG THE ACC

Argo floats drift with the ocean currents at typically 1,000 m depth, collecting vertical profiles of temperature and salinity between 2,000 m depth and the sea surface every 10 days[28]. Deployed from ships since 2001, the Argo network provides an almost continuous spatial coverage of the previously sparsely sampled Southern Ocean (Fig. 1). A comparison of the individual Argo profiles with the climatological mean state, as provided by the recent hemispheric extension of the high-resolution CSIRO Atlas of Regional Seas (CARS (ref. 29)), shows a conspicuous

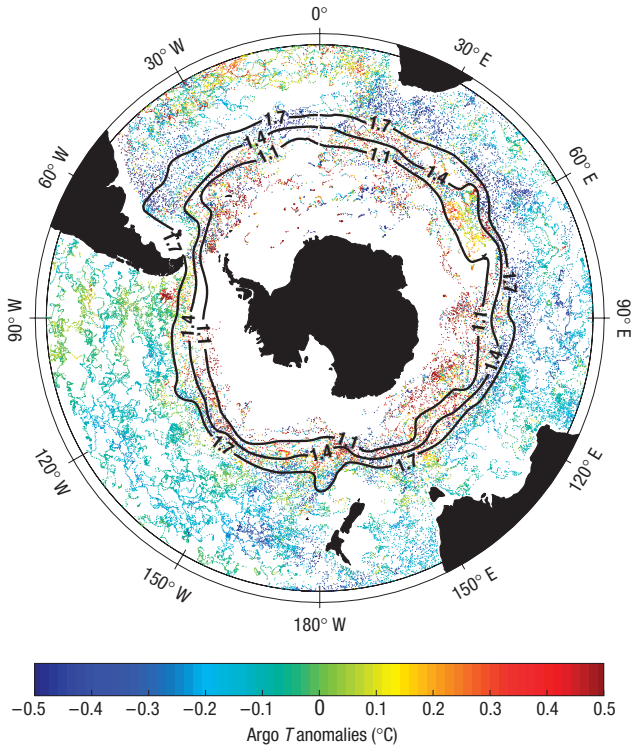


**Figure 1 Spatial pattern of changes in the ACC.** The dots show the distribution of the 52,447 Argo profiles used in this study. The colour indicates the deviations of Argo potential temperatures averaged over the neutral-density layer 26.9–27.7 from the climatological mean, gridded atlas values of CARS. Dark curves are contours (1.1, 1.4 and 1.7 m, from south to north) of climatological dynamic height (0/2,000 dbar), giving an approximate representation of ACC position. The branches of the ACC associated with the PF and SAF are located in the vicinity of the 1.4- and 1.7-m-dynamic-height contours over most of the domain.

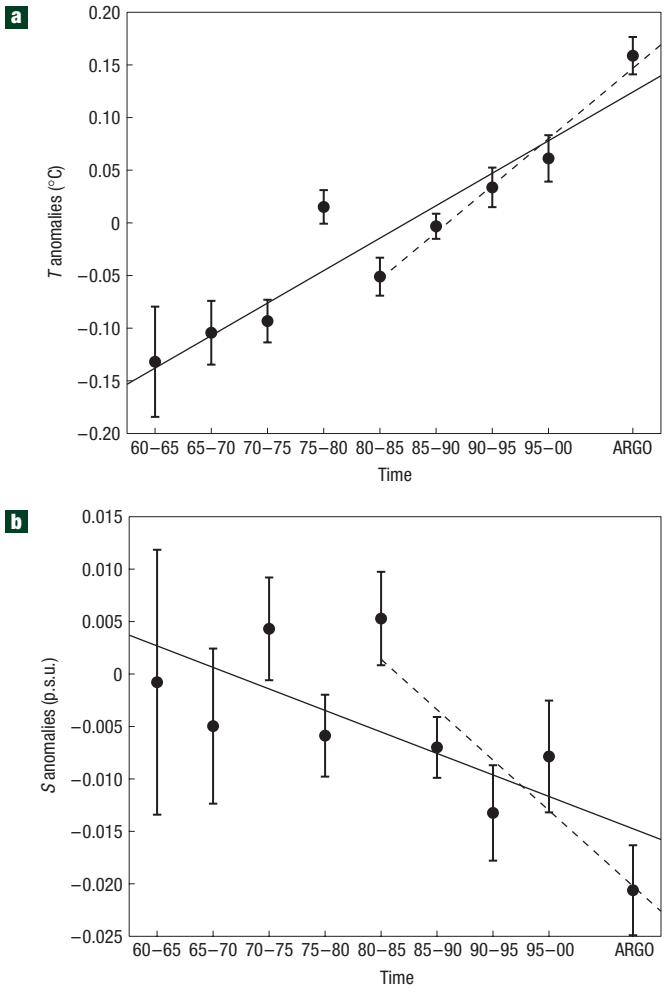


**Figure 2 Temporal evolution of potential temperature and salinity within the ACC. a**,**b**, Pentadal anomalies of $T$ (**a**) and $S$ (**b**), obtained from the deviations of individual casts from the long-term climatological mean values of CARS, hemispherically averaged between dynamic-height contours of 1.06–1.78 m (corresponding to mean latitudes of 54.6° S and 46.2° S), and between 300 and 1,000 m depth. Regression lines represent the linear trend since 1960 (dashed: since 1980). Error bars represent 95%-confidence intervals, representing the uncertainty due to short-term variability and random measurement errors.

pattern of change relative to the historic database: averaged over the isopycnal layer $\gamma = 26.9$–$27.7$ ($\gamma$ denoting neutral density[30]), which comprises the bulk of the water masses of the ACC, the waters on the poleward flank of the ACC have become warmer (and, equivalently, more saline) in this density layer, whereas a reversed tendency of cooling/freshening can be observed on the equatorward side. The anomalies show two intriguing features: they are oriented along the course of the ACC, approximately given by the contours of constant dynamic height (0/2,000 dbar), and they seem remarkably uniform along these streamlines, with no significant differences between the Atlantic, Indian, and Pacific sectors. To assess the structure of temporal changes across the ACC in a mean sense, we make use of this behaviour by examining averages along dynamic-height bins.

## TEMPORAL EVOLUTION OF CHANGES IN THE ACC

The temporal evolution of the hydrographic properties is assessed by comparing the Argo measurements of potential temperature ($T$) and salinity ($S$) with the historic database for the decades of the 1960s, 1970s, 1980s and 1990s. Sampling points have varied between these decades and temporal mean fields change along the course of the ACC; hence, spatial aliasing can occur in bin-averaged decadal differences. Adopting the approach of previous studies[31,32], this effect can be minimized by subtracting the temporal mean state from each profile; as an approximation of the unknown temporal mean, we use here the climatological mean fields of CARS to calculate these anomaly profiles.

The temporal evolution of the hydrographic properties in the ACC is assessed by considering averages of $T$ and $S$ anomalies over a relatively broad (~500-km-wide) and thick (300–1,000 m) swath of dynamic heights spanning the polar front (PF) and subantarctic front (SAF); in this way enough historic casts are retained to enable an inspection of pentadal mean values (Fig. 2). The temporal changes were dominated by multidecadal warming and freshening trends since the 1960s. In the temperature evolution there is some indication for an increase in the pace of change since the 1980s. The linear rate of warming was $0.006 \pm 0.001\,^{\circ}\mathrm{C\,yr^{-1}}$ over the full period, increasing to $0.009 \pm 0.001\,^{\circ}\mathrm{C\,yr^{-1}}$ for the latter period. The pentadal salinity anomalies involve relatively large error bars for the 1960s, rendering the trend over the full period only marginally significant ($-0.0004 \pm 0.0003\,\mathrm{yr^{-1}}$); however, the freshening stands

out since the 1970s or 1980s ($-0.0010 \pm 0.0004\,\mathrm{yr}^{-1}$ for the latter period).

## TRENDS IN WATER-MASS PROPERTIES ON ISOPYCNAL SURFACES

Repeat hydrographic transects in the Indian and western Pacific sectors of the Southern Ocean have suggested changes both in the upper Circumpolar Deep Water (UCDW) upwelling regime south of the ACC and in the Antarctic Intermediate and Subantarctic Mode Waters, which ventilate the thermocline north of the ACC: the regional water-mass properties on constant-density surfaces have been characterized by trends since the 1960s towards warm and saline anomalies for the UCDW south of the PF (ref. 31) and to cool and fresh anomalies in the lower thermocline waters exported from the Southern Ocean[32–36].

We assess the hemispheric-scale, linear trend of water-mass properties on neutral-density surfaces by averaging the anomalies along dynamic height bins of about 0.09 m. The trend shows two distinct patterns (Fig. 3). The dense (UCDW) water on the poleward side of the ACC has become warmer, with maximum trends of $0.017 \pm 0.004\,^{\circ}\mathrm{C\,yr}^{-1}$ around $\gamma = 27.5$ (equivalent to a salinization trend of $0.064 \pm 0.015\,\mathrm{yr}^{-1}$). In the thermocline north of the PF, above the layer of minimum salinity defining the core of Antarctic Intermediate Waters (near $\gamma = 27.3$), widespread cooling has occurred, with a trend of $-0.012 \pm 0.005\,^{\circ}\mathrm{C\,yr}^{-1}$ at $\gamma = 27.1$–$27.2$ (equivalent to a freshening of $-0.045 \pm 0.020\,\mathrm{yr}^{-1}$). The observed warming/cooling (or, equivalently, salinization/freshening) pattern on density surfaces across the ACC is similar to the trends obtained in model simulations of climate change during the past century, which were identified as a 'fingerprint' of anthropogenic changes in the air–sea fluxes of heat and fresh water[37].

## TEMPERATURE AND SALINITY TRENDS ON ISOBARIC SURFACES

While property changes on density surfaces are indicative of altered heat and freshwater fluxes at the sea surface[38], changes on isobaric surfaces can also be due to adiabatic movements of water masses, as caused by wind-driven changes in the circulation and mesoscale eddy variability. Despite the larger noise on isobars, coherent patterns of large-scale temperature and salinity change across the ACC can be discerned (Fig. 4): a wedge of warming slanting down along density surfaces, with a maximum at $\gamma = 27.2$–$27.4$, extending from the surface layer polewards of the PF to depths of more than 1,200 m at the SAF. (As discussed in previous studies[33,38], a subduction of warmer surface waters is consistent with a cooling on isopycnal surfaces, as observed for the lower Subantarctic Mode Water layer in Fig. 3; for further discussion see Supplementary Information, Fig. S1.) The latitudinal distribution of the mid-depth signal is consistent with previous observations on the basis of (non-profiling, ALACE) float measurements in the 1990s (ref. 26) (Fig. 4c). The trend around 900 m depth between the 1960s and the Argo period was $0.0080 \pm 0.0025\,^{\circ}\mathrm{C\,yr}^{-1}$, essentially the same as the pre-1990s warming inferred from the ALACE measurements[26]. An intriguing feature of the upper-ocean distribution is the occurrence of strongest warming rates in the southern portion of the ACC: a similar meridional structure of warming is found in model simulations, caused by a wind-induced increase in poleward eddy heat flux that tends to exceed the effect of increased equatorward Ekman transport[21,22,39].

The spatial pattern of the salinity trend (Fig. 4b) is dominated by a broad-scale freshening of thermocline waters across the ACC. The strongest changes occurred in a layer ($\gamma = 27.0$–$27.1$) corresponding to the deep portion of the Subantarctic Mode Waters, generally consistent with the observations along individual,

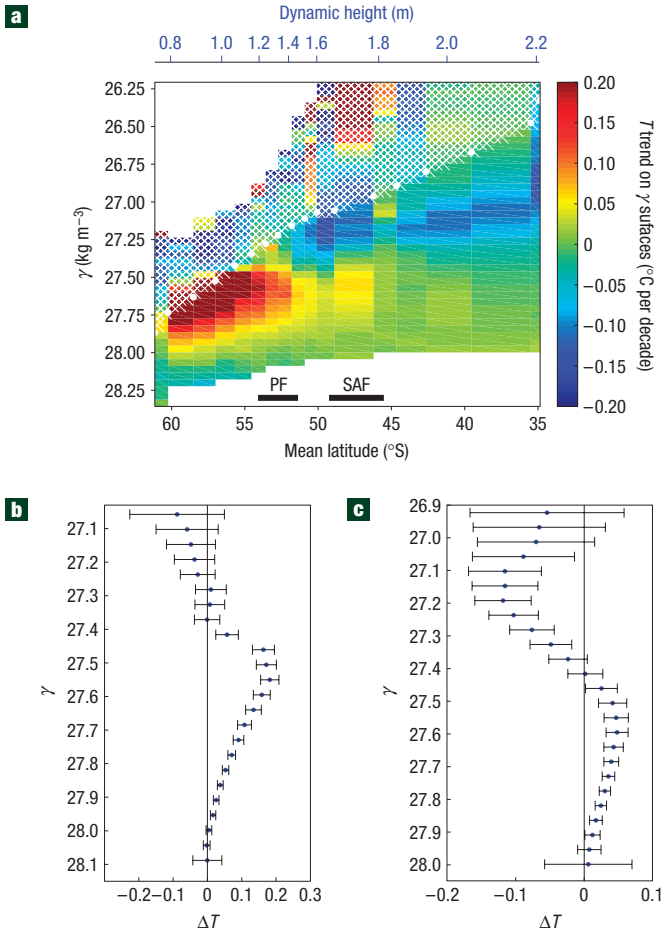


**Figure 3 Change of water-mass properties on isopycnal surfaces. a**, Mean decadal trend of potential temperature since the 1960s (°C per decade) on neutral-density surfaces, averaged along bins of ~0.09 m (indicated at the top), remapped onto latitude circles using the average latitudes of the dynamic-height contours. The white dots indicate the averaged density at 200 m depth, illustrating the vertical extent of the surface layer. Black bars indicate the average latitudes of the PF and SAF, corresponding to the ACC transport maxima in Fig. 4. **b**,**c** The trend as a function of neutral density for the dynamic-height ranges of 1.1–1.3 m and 1.5–1.7 m, respectively. Error bars denote 95%-confidence intervals, representing the uncertainty of the mean trends due to random, short-term variability.

repeat ship tracks from the South Indian and Pacific Ocean[31,32]. Although the error bars on the estimated salinity changes are relatively large (Fig. 4d), the uniform freshening over the whole latitudinal extent of the ACC stands out as a robust feature, irrespective of whether the trends are calculated since the 1960s or the 1980s. The structure of the freshening signal suggests a response to decreased salinities in the surface source regions, consistent with the increase in precipitation poleward of ~45° S projected by model simulations of twentieth-century climate change[40].

## STRUCTURE OF DENSITY TRENDS ACROSS THE ACC

What are the implications of the observed warming and freshening trends for the density structure, and hence the circulation? The primary signal in the observed density trend across the ACC is a broad-scale subsidence of isopycnal ($\gamma$) surfaces (Fig. 4a): over the PF–SAF at 800–1,000 m it exceeded 50 m over the

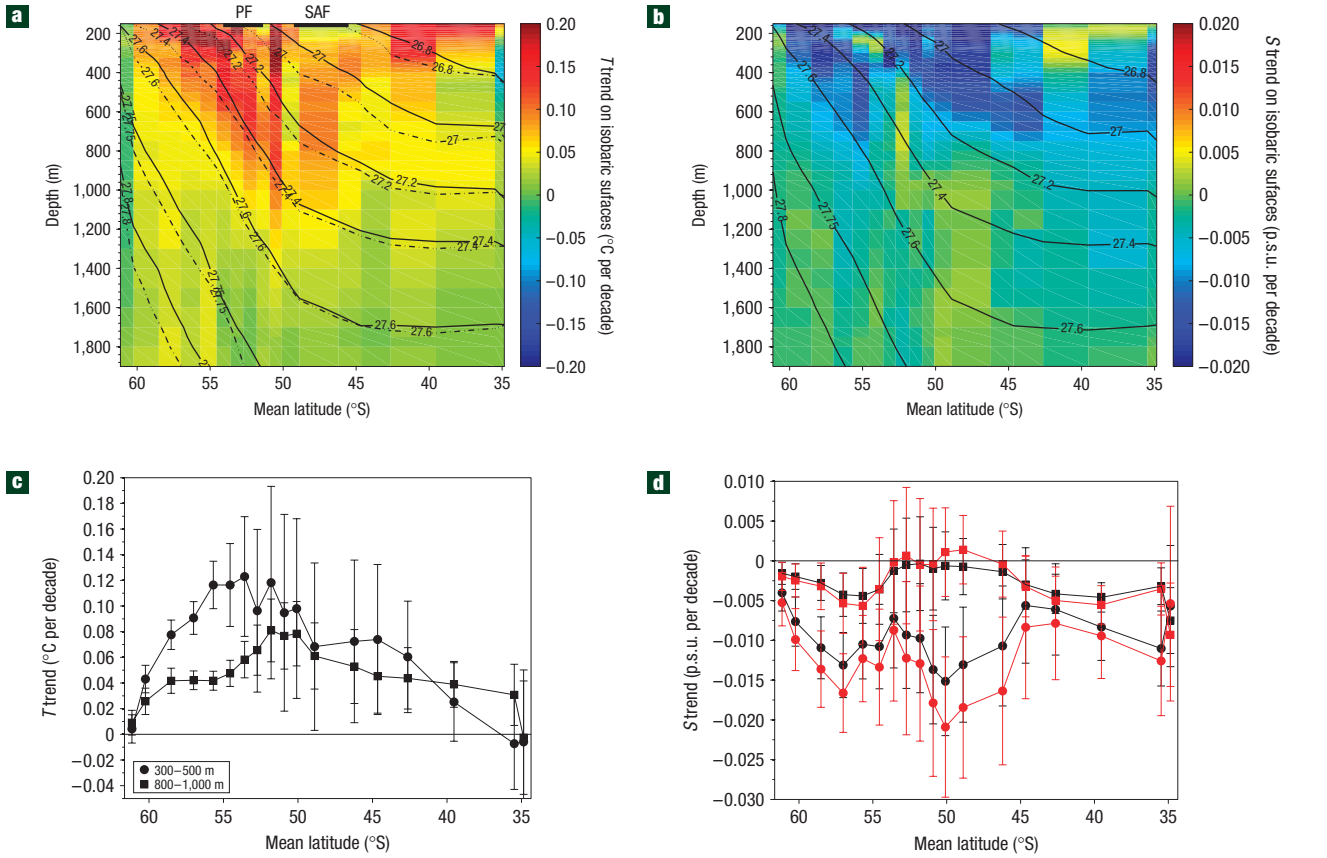


**Figure 4 Temperature and salinity changes across the ACC. a**,**b**, Mean decadal trends as in Fig. 3, but averaged on isobaric surfaces, of potential temperature (**a**) and salinity (**b**). Black contours in **a** illustrate the migration of isopycnal surfaces during the past four decades: continuous (dashed) curves represent potential densities obtained by subtracting (adding) the linear trends over two decades from (to) the climatological values of CARS. Black contours in **b** denote the mean climatological isopycnal surfaces given by CARS. **c**, The latitudinal distribution of the *T* trend (in °C per decade) for two depth ranges; **d**, the distribution of the *S* trend (per decade), alternatively calculated for the period since 1960 (black), and since 1980 (red). Error bars represent 95%-confidence intervals.

past 40 years; this is equivalent to southward displacements of about 50–80 km, consistent with previous inferences from individual sections[26,31]. However, this shift was not accompanied by a systematic increase in the tilt of isopycnals, or equivalently in the meridional density gradient across the ACC: although there was a slight steepening of isopycnals below 500 m reflecting the mid-depth warming/freshening maxima near the SAF, a reverse tendency occurred in near-surface layers owing to the concentration of warming/freshening in the southern portion of the ACC (Supplementary Information, Fig. S2).

Owing to the nature of geostrophic flow, the density contrast across the current is closely linked to the overall transport[15]. A direct measure of the baroclinic ACC transport is provided by the gradient of the potential-energy anomaly (PEA (refs 16,41,42)). The north–south difference in mean PEA (Fig. 5a) corresponds to a baroclinic transport above 1,900 m of 81 Sv (about two-thirds of the total ACC transport), with a concentration between the dynamic-height contours of 1.2 and 1.8 m, equivalent to mean latitudes of 53° and 45° S, respectively; the two transport maxima are indicative of the ACC branches associated with the PF and SAF. The change in PEA (Fig. 5b) is characterized by a rather uniform increase over the bulk of the ACC, north of ~57° S. The increase in the PEA gradient south of 57° S corresponds to an increase of ~2 Sv of eastward transport; however, because a relatively large fraction of the density trends near 60° S is due to the changes in salinity, estimates of meridional density gradients in this southern portion become less robust than further north.

## IMPLICATIONS FOR ACC DYNAMICS

Studies on the basis of coarse-resolution ocean models suggest that the enhanced equatorward Ekman transport associated with a poleward shift and intensification of the Southern Hemisphere westerlies (a positive trend in the Southern Annular Mode index) results in an increased circulation in the subpolar meridional overturning cell[16,17], implying an increased upwelling of deep water rich in dissolved inorganic carbon south of the circumpolar flow[10–12,43,44]. A reduction in the Southern Ocean $CO_2$ uptake relative to expectations from atmospheric $CO_2$ levels was inferred from an inversion of atmospheric observations[45–48] and attributed to an increase in outgassing of natural carbon dioxide as a result of this mechanism.

However, none of the ocean models used to study the response of the ACC and Southern Ocean carbon sink to changes in wind forcing resolve eddies. Observations suggest that stronger westerly winds induce, with a lag of 2–3 years, an increase in eddy activity[25]. High-resolution models that do resolve eddies capture this effect and suggest that the associated eddy fluxes could compensate the

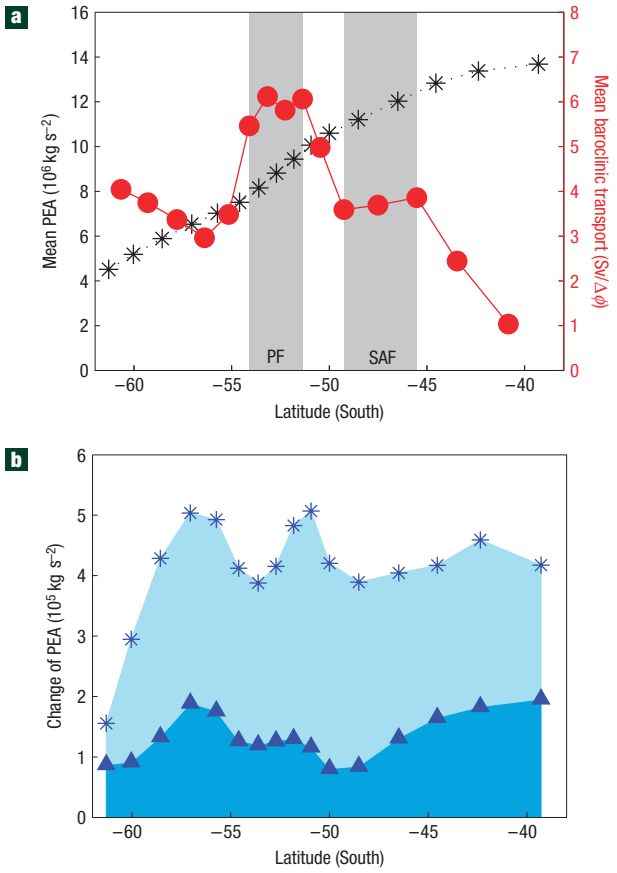


**Figure 5 Trend in baroclinic potential-energy anomaly and volume transport.** **a**, Distribution of mean baroclinic PEA (black asterisks) for the upper 1,900 m on the basis of climatological (CARS) *T* and *S* fields, and mean baroclinic transport of the ACC (in Sv per degree latitude) (red circles) derived from the meridional gradient of PEA. **b**, Change of PEA over the past four decades on the basis of the linear trends in *T* and *S*; triangles and the dark-blue shaded area denote the individual effect of the trend in *S*, light blue the individual effect of the trend in *T*. All fields are averaged along dynamic-height bins, remapped to the mean latitudes.

initial increases in northward Ekman transport[20–22]. As a result, the upwelling, isopycnal tilt and ACC transport tend to be insensitive (on timescales longer than a few years) to changes in wind forcing, a behaviour not found in coarse-resolution models using a standard parameterization of eddy effects[49].

Our analysis of trends in the physical properties suggests two main conclusions about the nature of ongoing changes in the ACC. First, as shown by the prominent patterns of change on isopycnal surfaces, significant parts of the mid-depth warming and freshening signals must be due to trends in surface heat and freshwater fluxes: the observed patterns of change are consistent with the 'fingerprint' of anthropogenic climate change delineated in model simulations[37]. Second, the lack of an increase in the tilt of isopycnals and in the transport of the ACC is not consistent with the response to the trend in the Southern Annular Mode index simulated by coarse-resolution models: the observed behaviour rather suggests a strong effect of wind-induced increases in eddy fluxes as found in eddy-resolving ocean models. Projecting the behaviour of the Southern Ocean, including the carbon sink, in greenhouse scenarios will thus require models that capture realistically the effect of the ACC eddy variability.

## METHODS

The domain of interest is the Southern Ocean south of 30° S. Measurements from areas with water depths less than 1,000 m were excluded to avoid effects of near-coastal and shelf processes. Historic casts taken during the 1960s (7,715 profiles), 1970s (9,483), 1980s (12,979) and 1990s (13,971) were compared with quality-controlled Argo profiles from 2002 to 2006. Data for the 1960s to 1990s are drawn from the BLUElink Ocean Archive (http://www.marine.csiro.au/~dunn/cars2006), a comprehensive Southern Ocean dataset assembled from all known sources[29,50], including WOD01, WOCE WHP3.0 and CSIRO holdings of Australian data; both bottle and conductivity–temperature–depth probes are used; expendable bathythermograph data are not included. All casts are interpolated onto a set of standard depth levels, with stringent quality control procedures involving a comprehensive screening for duplicates, poorly documented casts and outliers from background *T*–*S* fields.

The irregularly distributed profiles comprised by the BLUElink Ocean Archive constitute the basis for a high-resolution, gridded climatology of the Southern Ocean, originally referred to as CARS; in its recent update (CARS2006) it covers the world ocean from 70° S to 26° N, at a resolution of 0.5°. The mapping approach adapts to the data density by involving an interpolation of individual casts with a locally weighted least squares quadratic smoother; it thus provides a gridded estimate with higher resolution than simple spatial averaging used in other climatologies[50].

The quality of the Argo data was assessed by comparison with CARS. After initial screening of clear outliers, the Argo salinities were compared with climatological values on potential-temperature surfaces. CARS includes the r.m.s. salinity residuals as a function of potential temperature at each grid point (where the residual is the difference between the mean value and each cast contributing to the mean). Salinity values larger than three times the residual were rejected. Temperature and salinity profiles were then compared with climatology on pressure surfaces and outliers rejected. A total of 52,447 profiles passed the quality control procedure and were used in the analysis. As a further test, we compared the Argo profiles with high-quality conductivity–temperature–depth data taken along several meridional sections across the ACC during the same period. As shown in an example (the CLIVAR I8S section) included as Supplementary Information (Supplementary Information, Fig. S3), there is no significant difference in the *T*–*S* profiles from the two data sources.

A major source of error in estimating temporal changes from sparse ocean measurements arises from potential aliasing of differences in space, because sampling points differed from year to year. Following previous studies[31,32], we minimized the spatial aliasing arising from sampling points with different temporal mean fields by subtracting the temporal mean state from each profile. As an approximation to the unknown mean field during the observation period, we used the CARS climatology for deriving *T* and *S* anomaly profiles from each of the individual BLUElink Ocean Archive and Argo profiles.

A prime characteristic of the horizontal distribution of the anomaly fields (Fig. 1) in the Southern Ocean is their orientation along the course of the ACC, as approximately given by the contours of mean dynamic height (0/2,000 dbar). To analyse the structure of the temporal changes across the ACC, the anomaly profiles were thus sorted into bins of constant dynamic height, along which hemispheric averages were taken. Compared with approaches that involve differencing collocated profiles, for example pairs of observations within 220 km distance irrespective of their orientation relative to the stream axis[27], the present methodology involves less smoothing across the ACC.

A source of error in the computation of long-term changes is contamination by short-term variability, in particular seasonal variability near the sea surface and mesoscale eddy variability in the ocean interior. As shipboard data have been taken mainly during austral summer, these do not resolve the seasonal cycle. Hence no inferences about longer-term trends are possible for the surface layer, which we conservatively take to be the upper 200 m. The effect of random sampling errors (to which, below the surface layer, eddy noise is the main contributor) on the mean values was estimated by calculating 95%-confidence intervals, given by doubling the population standard deviation (obtained from Argo) divided by the square root of the number of degrees of freedom of the sample; the latter is approximated by half the number of profiles used for the bin averaging, accounting for the possibility of some non-zero correlations between successive profiles (that is, the possibility that individual eddies may have influenced more than one cast). Another potential source of error is the effect of irregular sampling with time (for example different spatial sampling in different decades). The large-scale consistency of the trends supports the conclusion that the temporal sampling is adequate to resolve hemispheric

trends. We also examined in detail particular regions that are well sampled throughout the period considered and found that the results agreed with the inferred large-scale trends.

Received 13 August 2008; accepted 28 October 2008; published 23 November 2008.

## References


1. Rintoul, S. R., Hughes, C. W. & Olbers, D. in *Ocean Circulation & Climate* (eds Siedler, G., Church, J. & Gould, J.) 271–302 (Academic, 2001).
2. IPCC, *in Climate Change 2007: The Physical Science Basis. Contribution of Working Group I to the Fourth Assessment Report of the Intergovernmental Panel on Climate Change* (eds Solomon, S., *et al.*) 1009 (Cambridge Univ. Press, 2007).
3. Toggweiler, J. R. & Russell, J. Ocean circulation in a warming climate. *Nature* **451**, 286–288 (2008).
4. Levitus, S., Antonov, J., Boyer, T. P. & Stephens, C. Warming of the world ocean. *Science* **287**, 2225–2229 (2000).
5. Barnett, T. P. *et al*. Penetration of human-induced warming into the world's oceans. *Science* **309**, 284–287 (2005).
6. Levitus, S., Antonov, J. & Boyer, T. Warming of the world ocean. *Geophys. Res. Lett.* **32**, L02604 (2005).
7. Willis, J. K., Roemmich, D. & Cornuelle, B. Interannual variability in upper ocean heat content, temperature, and thermosteric expansion on global scales. *J. Geophys. Res.* **109**, doi:10.1029/2003JC002260 (2004).
8. Sabine, C. L. *et al*. The oceanic sink for anthropogenic $CO_2$. *Science* **305**, 367–371 (2004).
9. Mikaloff Fletcher, S. E. *et al.* Inverse estimates of anthropogenic $CO_2$ uptake, transport, and storage by the ocean. *Glob. Biogeochem. Cycles* **20**, doi:10.1029/2005GB002530 (2005).
10. Zickfeld, K., Fyfe, J. C., Saenko, O. A., Eby, M. & Weaver, A. J. Response of the global carbon cycle to human-induced changes in the Southern Hemisphere winds. *Geophys. Res. Lett.* **34**, doi:10.1029/2006GL028797 (2007).
11. Lenton, A. & Matear, R. J. Role of the Southern Annular Mode (SAM) in Southern Ocean $CO_2$ uptake. *Glob. Biogeochem. Cycles* **21**, GB2016 (2007).
12. Lovenduski, N. S., Gruber, N. & Doney, S. C. Toward a mechanistic understanding of the decadal trends in the Southern Ocean carbon sink. *Glob. Biogeochem. Cycles* **22**, doi:10.1029/2007GB003139 (2008).
13. Fyfe, J. C. & Saenko, O. A. Simulated changes in extratropical Southern Hemisphere winds and currents. *Geophys. Res. Lett.* **33**, L06701 (2006).
14. Yin, J. H. A consistent poleward shift of the storm tracks in simulations of 21st century climate. *Geophys. Res. Lett.* **32**, L18701 (2005).
15. Bi, D., Budd, W. F., Hirst, A. C. & Wu, X. Response of the Antarctic Circumpolar Current transport to global warming in a coupled model. *Geophys. Res. Lett.* **29**, doi:10.1029/2002GL015919 (2002).
16. Saenko, O. A., Fyfe, J. C. & England, M. H. On the response of the oceanic wind-driven circulation to atmospheric $CO_2$ increase. *Clim. Dyn.* **25**, 415–426 (2005).
17. Hall, A. & Visbeck, M. Synchronous variability in the Southern Hemisphere atmosphere, sea ice, and ocean resulting from the annular mode. *J. Clim.* **15**, 3043–3057 (2002).
18. Oke, P. R. & England, M. H. Oceanic response to changes in the latitude of the Southern Hemisphere subpolar westerly winds. *J. Clim.* **17**, 1040–1054 (2004).
19. Sen Gupta, A. & England, M. H. Coupled ocean–atmosphere–ice response to variations in the Southern Annular Mode. *J. Clim.* **19**, 4457–4486 (2006).
20. Hallberg, R. & Gnanadesikan, A. The role of eddies in determining the structure and response of the wind-driven Southern Hemisphere overturning: Initial results from the Modelling Eddies in the Southern Ocean project. *J. Phys. Oceanogr.* **36**, 3312–3330 (2006).
21. Hogg, A. McC., Meredith, M. P., Blundell, J. R. & Wilson, C. Eddy heat flux in the Southern Ocean: Response to variable wind forcing. *J. Clim.* **21**, 608–620 (2008).
22. Screen, J. A., Gillett, N. P., Stevens, D. P., Marshall, G. J. & Roscoe, H. K. The role of eddies in the Southern Ocean temperature response to the Southern Annular Mode. *J. Clim.* (in the press, 2008).
23. Thompson, D. W. L. & Solomon, S. Interpretation of recent Southern Hemisphere climate change. *Nature* **296**, 895–899 (2002).
24. Marshall, G. J. Trends in the Southern Annular Mode from observations and reanalyses. *J. Clim.* **16**, 4134–4143 (2003).
25. Meredith, M. P. & Hogg, A. M. Circumpolar response of Southern Ocean eddy activity to a change in the Southern Annular Mode. *Geophys. Res. Lett.* **33**, doi:10.1029/2006GL026499 (2006).
26. Gille, S. T. Warming of the Southern Ocean since the 1950s. *Science* **295**, 1275–1277 (2002).
27. Gille, S. T. Decadal-scale temperature trends in the Southern Hemisphere. *J. Clim.* **21**, 4749–4765 (2008).
28. Roemmich, D. *et al.* in *Observing the Oceans in the 21st century* (eds Koblinsky, C. J. & Smith, N. R.) 248–258 (GODAE Project Office and Bureau of Meteorology, 2001).
29. Ridgway, K. R., Dunn, J. R. & Wilkin, J. L. Ocean interpolation by four-dimensional weighted least squares—application to the waters around Australia. *J. Atmos. Oceanic Tech.* **19**, 1357–1375.
30. Jackett, D. R. & McDougall, T. J. A neutral density variable for the world's ocean. *J. Phys. Oceanogr.* **27**, 237–263 (1997).
31. Aoki, S., Bindoff, N. L. & Church, J. A. Interdecadal water mass changes in the Southern Ocean between 30° E and 160° E. *Geophys. Res. Lett.* **32**, L07607 (2005).
32. Wong, A. P. S., Bindoff, N. L. & Church, J. A. Freshwater and heat changes in the North and South Pacific oceans between the 1960s and 1985–94. *J. Clim.* **14**, 1613–1633 (2001).
33. Bindoff, N. L. & McDougall, T. J. Decadal changes along an Indian Ocean section at 32° S and their interpretation. *J. Phys. Oceanogr.* **30**, 1207–1222 (2000).
34. Bryden, H. L., McDonagh, E. L. & King, B. A. Changes in ocean water mass properties: Oscillations or trends? *Science* **300**, 2086–2088 (2003).
35. Bindoff, N. L. & Church, J. A. Warming of the water column in the southwest Pacific Ocean. *Nature* **357**, 59–62 (1992).
36. Johnson, G. C. & Orsi, A. H. Southwest Pacific Ocean water-mass changes between 1968/69 and 1990/91. *J. Clim.* **10**, 306–316 (1997).
37. Banks, H. T. & Bindoff, N. L. Comparison of observed temperature and salinity changes in the Indo–Pacific with results from the coupled climate model HadCM3: Processes and mechanisms. *J. Clim.* **16**, 156–166 (2003).
38. Bindoff, N. L. & McDougall, T. J. Diagnosing climate change and ocean ventilation using hydrographic data. *J. Phys. Oceanogr.* **24**, 1137–1152 (1994).
39. Fyfe, J. C., Saenko, O. A., Zickfeld, K., Eby, M. & Weaver, A. J. The role of poleward-intensifying winds on Southern Ocean warming. *J. Clim.* **20**, 5391–5400 (2007).
40. Held, I. M. & Soden, B. J. Robust responses of the hydrological cycle to global warming. *J. Clim.* **19**, 5686–5699 (2006).
41. Borowski, D., Gerdes, R. & Olbers, D. Thermohaline and wind forcing of a circumpolar channel with blocked geostrophic contours. *J. Phys. Oceanogr.* **32**, 2520–2540 (2002).
42. Rintoul, S. R., Sokolov, S. & Church, J. A 6 year record of baroclinic transport variability of the Antarctic Circumpolar Current at 140° E derived from expendable bathythermograph and altimeter measurements. *J. Geophys. Res.* **107**, doi:10.1029/2001JC000787 (2002).
43. Lovenduski, N. S., Gruber, N., Doney, S. C. & Lima, I. D. Enhanced $CO_2$ outgassing in the Southern Ocean from a positive phase of the Southern annular Mode. *Glob. Biogeochem. Cycles* **21**, GB2026 (2007).
44. Verdy, A., Dutkiewicz, S., Follows, M. J., Marshall, J. & Czaja, A. Carbon dioxide and oxygen fluxes in the Southern Ocean: Mechanisms of interannual variability. *Glob. Biogeochem. Cycles* **21**, GB2020 (2007).
45. Le Quéré, C. *et al*. Saturation of the Southern Ocean $CO_2$ sink due to recent climate change. *Science* **316**, 1735–1738doi:10.1126/science.1136188 (2007).
46. Law, R. M., Matear, R. J. & Francey, R. J. Comment on 'Saturation of the Southern Ocean $CO_2$ sink due to recent climate change'. *Science* **319**, 570a (2008).
47. Zickfeld, K., Fyfe, J. C., Eby, M. & Weaver, A. J. Comment on 'Saturation of the Southern Ocean $CO_2$ sink due to recent climate change'. *Science* **319**, 570b (2008).
48. Le Quéré, C. *et al*. Response to comments on 'Saturation of the Southern Ocean $CO_2$ sink due to recent climate change'. *Science* **319**, 570c (2008).
49. Gent, P. R. & McWilliams, J. C. Isopycnal mixing in ocean circulation models. *J. Phys. Oceanogr.* **20**, 150–155.
50. Dunn, J. R. & Ridgway, K. R. Mapping ocean properties in regions of complex topography. *Deep-Sea Res. I* **49**, 591–604 (2002).


Supplementary Information accompanies the paper at www.nature.com/naturegeoscience.

## Acknowledgements

We acknowledge the role of J. Dunn in developing and making available the CSIRO ocean data archives, and K. Lorbacher for her assistance in the data analysis. The study was initiated during visits of C.W.B. and A.D. at CSIRO Marine Research Laboratories in Hobart, supported by an Ernst Froehlich Fellowship (C.W.B.) and a grant from DAAD (A.D.). This research was supported in part by the CSIRO Wealth from Oceans Flagship, the Australian government's Cooperative Research Centre (CRC) programme through the ACE CRC, and the Australian Greenhouse Office. The paper is a contribution to The Future Ocean Cluster at Kiel University.

## Author information

Reprints and permissions information is available online at http://npg.nature.com/reprintsandpermissions. Correspondence and requests for materials should be addressed to C.W.B.